Nonlinear Controller for MMC-HVdc Operating in Grid-Forming Mode

Luís Lourenço, Alessio Iovine, Gilney Damm, Alfeu Filho

Nonlinear Controller for MMC-HVDC Operating in Grid-Forming Mode

Luís F. Normandia Lourenço, *Member, IEEE*, Alessio Iovine, *Member, IEEE*, Gilney Damm, *Member, IEEE*, and Alfeu J. Sguarezi Filho, *Senior Member, IEEE*

***Abstract*—The development of the Modular Multilevel Converter (MMC) enabled the efficient creation of high-power High Voltage Direct Current (HVDC) transmission systems. As a result, MMC-HVDC transmission systems became the main alternative to integrate remote renewable energy sources being deployed in accelerating rates to fight climate change. As the number of online classical synchronous generators decreases while the one of converter-based power sources increases, power systems are suffering from lower inertia levels and from fewer providers of ancillary services. Therefore, new control strategies, such as the Grid-Forming (GFM) converter operation, were developed to address the ongoing power system transformation. The main contribution of the present paper is to propose a nonlinear control strategy compatible with GFM operation for an MMC-HVDC transmission system controlled as a Virtual Synchronous Machine (VSM). The control strategy is developed using nonlinear control tools such as feedback linearization, dynamic feedback linearization and backstepping. In addition, the present paper provides a rigorous mathematical stability analysis applying Lyapunov theory. The proposed control strategy is then validated by simulations using the Matlab/Simscape Electrical package in three situations: active power tracking, converter energy tracking and a frequency support scenario. Results show the good performance of the proposed nonlinear controller for all situations considered, presenting a fast response and a faster disturbance rejection compared to classical PI controller.**

***Index Terms*—Modular Multilevel Converter, HVDC, Nonlinear control, Lyapunov stability, Grid-forming Converter.**

NOMENCLATURE

$v_{u,j}, v_{l,j}$	MMC upper and lower arm voltages of phase $j = \{a, b, c\}$ or component $j = \{d, q, 0\}$ in per unit values (p.u.).
$i_{u,j}, i_{l,j}$	MMC upper and lower arm voltages of phase $j = \{a, b, c\}$ or component $j = \{d, q, 0\}$ in p.u..
$i_{s,j}$	MMC output current of phase $j = \{a, b, c\}$ or component $j = \{d, q\}$ in p.u..
$v_{g,j}$	Grid voltage of phase $j = \{a, b, c\}$ or component $j = \{d, q\}$ in p.u..
$i_{g,j}$	Grid current of phase $j = \{a, b, c\}$ or component $j = \{d, q\}$ in p.u..
$i_{cir,j}$	MMC circulating current of phase $j = \{a, b, c\}$ or component $\{j = d, q, 0\}$ in p.u..
r, l	MMC arm resistance and inductance in p.u..
r_g, l_g	Grid equivalent resistance and inductance in p.u..
r_f, l_f, c_f	Resistance, inductance and capacitance of the PoC filter in p.u..
r_{eq}, l_{eq}	Equivalent resistance and inductance.
$v_{f,j}$	PoC voltage of phase $j = \{a, b, c\}$ or component $j = \{d, q\}$ in p.u..
$e_{dif,j}$	Differential voltage of phase $\{j = a, b, c\}$ or component $j = \{d, q\}$ in p.u..
$e_{sum,j}$	Average voltage of phase $j = \{a, b, c\}$ or component $j = \{d, q\}$ in p.u..
v_{dc}	DC link voltage in p.u..
ω_b	System base value for frequency.
ω	Frequency of PoC voltage.
W	Converter energy in p.u..
W_Δ	Energy imbalance in p.u..
δ_g	Grid equivalent phase angle.
ω_g	Grid equivalent frequency deviation from a synchronous reference.
M_g	Grid equivalent inertia coefficient.
$P_{m,g}, P_{e,g}$	Grid equivalent mechanic and electric power.
P_L	Load power consumption.
δ_c	Grid-forming converter phase angle.
ω_c	Grid-forming converter frequency deviation from a synchronous reference.
M_v	Grid-forming virtual inertia coefficient.
$\overline{P}_c, P_{e,c}$	Grid-forming active power reference and electric power.
K_c	Grid-forming virtual damping coefficient.
δ	Phase difference between the grid and the grid-forming converter.
$\tilde{\omega}$	Frequency difference between the grid and the grid-forming converter.
S_b	Base value for power.
K_i, K_i^α	Controller proportional and integral gains.
α_i	Auxiliary state variable for the controller.
Ψ_i	Auxiliary controller input.
x	State variable.

This work was supported by the São Paulo Research Foundation FAPESP (grant#2021/10421-0 and #2023/00682-6), the National Council for Scientific and Technological Development CNPq (grant#407867/2022-8) and by the Agence Nationale de la Recherche (ANR) via grant ESTHER ANR-22-CE05-0016.

Luís F. Normandia Lourenço is with the Institue of Energy and Environment, University of São Paulo (IEE-USP), 1289 Avenida Professor Luciano Gualberto, 05508-010, São Paulo, Brazil (e-mail: lourenco@iee.usp.br)

Alessio Iovine is with the CNRS and with the Laboratoire des Signaux et Systèmes (L2S), CentraleSupélec, Université Paris-Saclay, 91192 Gif-sur-Yvette, France (e-mail: alessio.iovine@centralesupelec.fr)

Gilney Damm is with COSYS-LISIS, Univ Gustave Eiffel, IFSTTAR, F-77447 Marne-la-Vallée, France (e-mail: gilney.damm@univ-eiffel.fr)

Alfeu J. Sguarezi Filho is with the Center for Engineering, Modeling and Applied Social Sciences (CECS), UFABC, 5001 Avenida do Estado, 09210-580, Santo André, Brazil (e-mail: alfeu.sguarezi@ufabc.edu.br)

$\overline{x}$	Set-point value of a state variable.
x^*	Trajectory of a state variable.
$\mathcal{V}_j$	Lyapunov function.

I. Introduction

TO tackle climate change, and allow increased energy independence, the power sector is moving towards environmental friendly renewable energy sources. The integration of these resources into the power grid poses a major challenge for system operators since they are often located far from the load centers, in remote locations, or even offshore. High Voltage Direct Current (HVDC) transmission based on Voltage Source Converters (VSC) emerged as a mature technology that would enable the interconnection of remote or offshore sites to the main grid [1], [2]. The transfer of power using VSC-HVDC has some advantages over its Line Commutated Converter counterpart that are crucial to the power system transformation such as the fast and independent control of active and reactive power and its ability to feed passive loads [3].

The Modular Multilevel Converter (MMC) proposed by [4], [5] became the favored VSC topology for HVDC systems [6], [7]. The modularity and scalability of this converter topology allowed for MMC-HVDC to reach high power and high voltage levels such as the 1 GW/400 kV DC Spain-France interconnection [8]. Moreover, they are more efficient than traditional 2-level VSC, a desired characteristic for high power applications [9] and, if a high enough number of submodules is adopted, their filters have a reduced size or could be even eliminated [10].

The urge to achieve a more sustainable power system through the proliferation of converter connected power sources such as large wind and solar farms and HVDC links creates a change within the very foundations of the power system. The power generation is displaced from conventional fossil fuel-based synchronous generators to non-synchronous generation resulting in power systems with reduced levels of inertia that put security and stability of supply at risk [11]. Additionally to this reduction in stability, fossil-fueled synchronous generators, which are the traditional providers of ancillary services to stabilize the grid, are being phased out to achieve the sustainable energy transition goals, thus reducing the capability of the power system to recover in the event of a disturbance without further grid support.

In the past decade, large low-inertia power systems were only seen as a theoretical possibility [12], however, system operators around the globe are currently expressing their concerns on the subject [13]–[15]. Nevertheless, the investigation of the August 9th, 2019, blackout event that occurred in England pointed the low level of inertia of the system and poorly tuned controllers as two of the major causes of the event [16]. Hence, to enable a sustainable energy transition with a stable and secure supply, it is necessary to develop control strategies that enable power converters that interface HVDC links to provide ancillary services to the grid tailored to the new challenges of power system operation [17].

A class of operation strategies for power converters that attracted researchers' attention in recent years is the Grid Forming Converter (GFM) [18], [19]. When a power converter operates as a GFM, it can impose a voltage waveform with its own phase angle, frequency and voltage amplitude. Therefore, it is able to provide new ancillary services to the grid such as virtual inertia and could even enable the operation without the presence of synchronous generators in a 100 % converter interfaced power system [20]–[22]. Within GFM operation, a wide number of strategies can be found such as the synchronverter [23], the Virtual Synchronous Machine (VSM) [24], [25], the hybrid angle control (HAC)[26], the dual port GFM [27] and the power angle-frequency droop [28].

The goal of the synchronverter control strategy [23] is to mimic the behavior of a Synchronous Generator (SG), intertwining the active and reactive power through the rotor excitation current (virtual), as it happens on real SG. The VSM presented in [24], [25] consists in using the swing equation of a SG to obtain the output voltage's frequency while the voltage's amplitude is given by a reactive power droop or by a fixed reference value. The HAC GFM method presented in [26] combines a DC-based matching control with a nonlinear angle feedback that resembles droop control. The study establishes parametric conditions for existence and uniqueness of solution, stability, and boundedness, achievable through careful selection of control parameters. In reference [27], a universal dual-port control strategy for GFM converters is proposed. The strategy goal is to form both converter AC and DC voltages, consolidating Grid-Following (GFL) and GFM functionalities into a single controller that is compatible with conventional machine-based generation systems. Reference [28] proposes a power angle-frequency droop control that uses an estimate of the converter power angle to determine its frequency. This method shows a similar performance with power-frequency droop in steady state operation whilst the transient stability margins are improved under current limitation.

The GFM strategies mentioned above [23]–[28] are ready to be deployed in 2-level VSCs as these works focus solely on the interaction of the converter with the electric grid. To demonstrate the suitability of these techniques to MMC-HVDC systems it is essential to consider the complex internal dynamics of the MMC system in future studies. These dynamics play a critical role in maintaining converter system stability and are intrinsically dependent on the AC side interactions. Therefore, they should be included to provide a better understanding of the interactions between the AC side dynamics and the internal converter dynamics.

Despite MMC being the favored topology for HVDC, only a few studies can be found on GFM MMCs [29]. In [30] a synchronous generator emulation control was proposed, where a swing equation was responsible for generating the phase angle and the frequency of voltage to be imposed at the point of connection. Ref. [31] proposed the control of the MMC as a synchronverter, using the well known dynamics of a synchronous generator to create the voltage's phase angle and amplitude. In [32], the authors suggested the operation of an MMC as a VSM with cascaded voltage and current control loops and validated the concept using an experimental setup. The operation of two MMC-HVDC links operating in parallel in GFM mode according to a power sharing droop strategy was

investigated by [33]. Nonetheless, these studies have focused only on the Alternating Current (AC) side dynamics and linear (PI) controllers, without addressing the internal MMC dynamics.

From the control system standpoint, the choice for the MMC topology adds the complex task of controlling its internal dynamics involving circulating currents, the converter energy and the energy balance. In [34], a thorough analysis of energy based control structures for a VSC-HVDC is conducted. The importance of the internal energy control for MMCs operating in GFM control was furthered investigated in [35], where the internal energy control is shown to be able to mitigate the interactions between the inner and outer control loops. Moreover, in [29] the buffering capability offered by the converter energy of an MMC is investigated when the converter is connected to an offshore wind farm or to an island grid. These works focused on linear techniques based on PI controllers and highlighted the importance of the converter energy control in GFM mode.

Obviously, also nonlinear control strategies have been investigated for MMC converters in the current literature. However, the focus so far has been on grid-following techniques. For instance, [36] presented a feedback linearization approach for controlling the circulating currents. In [37], a nonlinear control strategy for the internal MMC-HVDC dynamics is proposed. In [38], authors proposed a backstepping control method for MMCs that can be applied in both single and three-phase converters. Differently, Steckler *et al.* [39] formulated the MMC-HVDC control problem using differential flatness theory, but still targeting grid-following converter operation.

The present paper's contribution lies in the field of applied nonlinear control for MMCs, but focuses on GFM operation. Indeed, the main goal of this work is to propose a nonlinear control strategy for an MMC that is compatible with GFM operation and that explicitly controls the energy dynamics of the MMC. The proposed strategy based on feedback linearization and dynamic feedback linearization targets to improve the results obtained when using linear control techniques, and to contribute to the development of MMC-HVDC systems capable of supporting the electric grid with virtual inertia. A thorough stability analysis using Lyapunov theory is presented, showing that the closed loop system is asymptotically stable. The proposed control strategy is validated by simulations for an MMC-HVDC system connected to a power grid implemented using the Matlab/Simscape Electrical package.

Though it is shown in this work that the proposed MMC control strategy attains frequency support and synthetic inertia, automatically in a similar way a synchronous generator does, it is considered out of scope the design of dedicated ancillary services controllers, as frequency and voltage droop. Such control approaches among others will be developed in future works, based on the current results that provide a stable basis for such additional control layers. The proposed results then are an important step in the field of application of MMC based HVDC transmission systems for power system stabilization.

The remaining of the paper is organized as follows. Section II introduces the considered model for the MMC. Section III contains the adopted control laws and the reference trajectories for the dynamics. Section IV provides the stability analysis for the considered control laws. Section V describes numerical results, while Section VI provides conclusions.

II. System Modeling

Figure 1 shows a point-to-point HVDC transmission system with an MMC station controlled in GFM mode. When the inverter station is controlled in GFM mode, it generates a voltage waveform at the point of common coupling (PCC) with its own frequency, phase angle and amplitude. Ultimately, the control system compatible with GFM operation allows the converter to provide ancillary services to the grid such as frequency support and virtual inertial response [40].

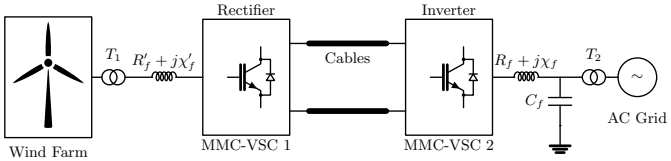

Fig. 1: Point to point MMC-HVDC link interconnecting an offshore wind farm.

Figure 2 shows the topology of the MMC-HVDC inverter station considered in this work. The MMC under study is composed of m identical half-bridge submodules connected in series, each of them composed of auto-commuted switches and a capacitor. The result is a converter with $N = 2m + 1$ levels. Each submodule can be controlled independently from each other. When a submodule is ON, the capacitor charges (or discharges) depending on the current signal and, when it is OFF, the capacitor is bypassed. These strings of submodules are placed in an arm of the converter and the two arms required for a phase are called a leg. Each leg's midpoint is connected to a smoothing reactor and a shunt capacitor filter.

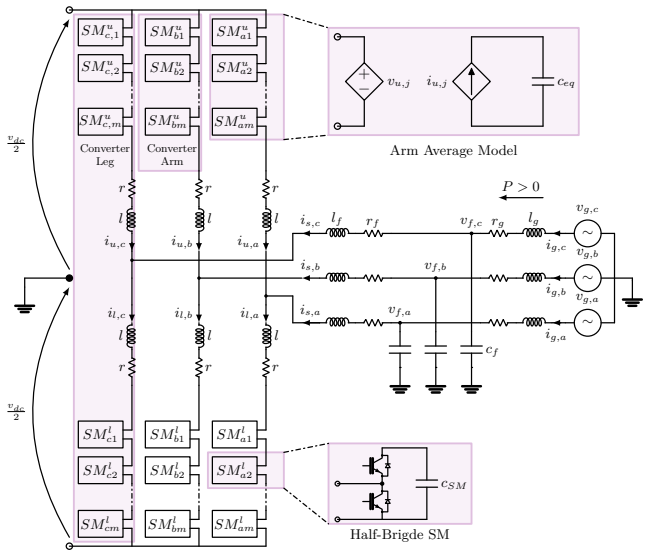

Fig. 2: Model of an MMC-HVDC station connected to the grid.

In Fig. 2, $v_{u,j}$ and $v_{l,j}$ are the voltages generated by the upper and lower arms, $i_{u,j}$ and $i_{l,j}$ are the currents of the upper and lower arms, $v_{g,j}$ is the grid equivalent voltage and

$v_{f,j}$ is the voltage at the PCC and $i_{s,j}$ is the converter output current, where $j = \{a, b, c\}$ indicates the phase. The model follows the passive sign convention. Then, active power is positive when flowing from the grid to the MMC station and it is negative when the HVDC system delivers active power to the grid.

For control purposes, an Arm Average Model (AAM) can be considered, where the string of submodules of each arm can be substituted by an equivalent voltage source (see [8], [10], [29], [34]). The control problem associated with the MMC operated in GFM mode is to generate a voltage waveform $v_{f,abc}$ at the converter terminals with its own frequency, amplitude and phase angle by manipulating the 6 converter arm equivalent voltages $v_{u,dq0}$, $v_{l,dq0}$ obtained in the synchronous reference frame. The control law should be able to regulate the power exchange between the converter and the AC grid and also to control the so-called internal MMC dynamics. To obtain a mathematical model of the MMC, the following definitions are considered:

$$i_{s,j} = -i_{u,j} + i_{l,j}, \qquad i_{cir,j} = \frac{1}{2}(i_{u,j} + i_{l,j}) \tag{1}$$

$$r_{eq} = r + 2r_f, \qquad l_{eq} = l + 2l_f \tag{2}$$

where $i_{s,j}$ is the output current and $i_{cir,j}$ is the circulating current. Throughout this work, the subscript j represents the components in the $dq0$ synchronous reference frame that is considered in the present paper; r and l are the resistance and inductance of the converter's arms; r_f and l_f are the resistance and the inductance of the smoothing filter; r_{eq} and l_{eq} are the equivalent resistance and inductance of the MMC.

Furthermore, we consider the following definitions of auxiliary inputs:

$$e_{dif,j} = v_{u,j} - v_{l,j} \tag{3}$$

$$e_{sum,j} = \frac{v_{u,j} + v_{l,j}}{2} \tag{4}$$

where the subscript j is $j = \{a, b, c\}$ or $j = \{d, q, 0\}$ depending on the context given by the reference frame adopted, $e_{dif,j}$ is an auxiliary input depending on the difference between $v_{u,j}$ and $v_{l,j}$, and $e_{sum,j}$ is an auxiliary input depending on the sum of $v_{u,j}$ and $v_{l,j}$. These definitions are made to simplify the MMC model and to avoid complex input determinations as in [37].

In the following subsections, the mathematical model of the MMC dynamics is presented.

A. Output Current

The output current is the current exchanged between the MMC and the electric grid. By applying the Kirchhof's Voltage Law to the circuit in Fig. 2 the following relations in per unit values can be obtained for the upper and lower arm of phase j as:

$$\frac{v_{dc}}{2} - v_{u,j} - ri_{u,j} - \frac{l}{\omega_b}\dot{i}_{u,j} + r_f i_{s,j} + \frac{l_f}{\omega_b}\dot{i}_{s,j} - v_{f,j} = 0 \tag{5}$$

$$-\frac{v_{dc}}{2} + v_{l,j} + ri_{l,j} + \frac{l}{\omega_b}\dot{i}_{l,j} + r_f i_{s,j} + \frac{l_f}{\omega_b}\dot{i}_{s,j} - v_{f,j} = 0 \tag{6}$$

where $\omega_b = 2\pi f$ is the grid frequency base constant value, with $f = 50Hz$ or $f = 60Hz$.

Adding (5) and (6), and substituting the definitions given in (1), (2) and (3):

$$\dot{i}_{s,j} = -\frac{\omega_b r_{eq}}{l_{eq}} i_{s,j} + \frac{\omega_b}{l_{eq}} e_{dif,j} + \frac{2\omega_b}{l_{eq}} v_{f,j} \tag{7}$$

In (7), the subscript j indicates the phases a, b and c. Then, the model in the synchronous reference frame is obtained by applying the following Park transformation (see [37], [41]):

$$\begin{bmatrix} x_d \\ x_q \\ x_0 \end{bmatrix} = \frac{2}{3} \begin{bmatrix} cos(\theta) & cos\left(\theta - \frac{2\pi}{3}\right) & cos\left(\theta + \frac{2\pi}{3}\right) \\ -sin(\theta) & -sin\left(\theta - \frac{2\pi}{3}\right) & -sin\left(\theta + \frac{2\pi}{3}\right) \\ \frac{1}{2} & \frac{1}{2} & \frac{1}{2} \end{bmatrix} \begin{bmatrix} x_a \\ x_b \\ x_c \end{bmatrix} \tag{8}$$

resulting in the per unit (p.u.) arm average model in the synchronous reference given by:

$$\dot{i}_{s,d} = -\frac{\omega_b r_{eq}}{l_{eq}} i_{s,d} + \omega\omega_b i_{s,q} + \frac{\omega_b}{l_{eq}} e_{dif,d} + \frac{2\omega_b}{l_{eq}} v_{f,d} \tag{9}$$

$$\dot{i}_{s,q} = -\omega\omega_b i_{s,d} - \frac{\omega_b r_{eq}}{l_{eq}} i_{s,q} + \frac{\omega_b}{l_{eq}} e_{dif,q} + \frac{2\omega_b}{l_{eq}} v_{f,q} \tag{10}$$

where ω is the voltage frequency in per unit values which will be generated by the GFM operation. Thus, ω is assumed as piece-wise constant for the electrical dynamics of the system.

B. Output Voltage

The output voltage is the voltage at the converter terminals. Its p.u. model is given by:

$$\dot{v}_{f,d} = \frac{\omega_b}{c_f}(i_{g,d} - i_{s,d}) + \omega\omega_b v_{f,q} \tag{11}$$

$$\dot{v}_{f,q} = \frac{\omega_b}{c_f}(i_{g,q} - i_{s,q}) - \omega\omega_b v_{f,d} \tag{12}$$

where the grid current $i_{g,dq}$ is a measured quantity in HVDC systems and, therefore, is considered as an exogenous input to the model.

C. Circulating Currents

Each converter arm voltage is obtained by turning ON a certain number of submodules. However, given the number of submodules and the balancing strategy, the submodules do not charge or discharge uniformly. As a consequence, there is a temporary voltage unbalance between the converter upper and lower arms and between the converter legs that generates the circulating currents.

To obtain the mathematical model for the circulating currents, the first step is to subtract (5) from (6):

$$\dot{i}_{cir,j} = -\frac{\omega_b r}{l} i_{cir,j} - \frac{\omega_b}{l} e_{sum,j} + \frac{\omega_b}{l} v_{dc} \tag{13}$$

In (13), the subscript j indicates the phases a, b and c. Then, the model in the synchronous reference frame is obtained by applying the Park transformation in (8), resulting in the p.u. mathematical model for the circulating currents $i_{cir,d}$, $i_{cir,q}$ and $i_{cir,0}$ given by:

$$\dot{i}_{cir,d} = -\tfrac{\omega_b r}{l} i_{cir,d} + \omega\omega_b i_{cir,q} - \tfrac{\omega_b}{l} e_{sum,d} \tag{14}$$

$$\dot{i}_{cir,q} = -\omega\omega_b i_{cir,d} - \tfrac{\omega_b r}{l} i_{cir,q} - \tfrac{\omega_b}{l} e_{sum,q} \tag{15}$$

$$\dot{i}_{cir,0} = -\tfrac{\omega_b r}{l} i_{cir,0} - \tfrac{\omega_b}{l} e_{sum,0} + \tfrac{\omega_b}{l} v_{dc} \tag{16}$$

D. Converter Energy

Converter energy refers to the energy stored in the capacitor of every submodule. When the model is obtained in the $dq0$ frame, there are two important energy quantities: the converter total energy W that is the sum of the energy stored in all submodules; and the converter energy difference W_Δ that is the difference between the energy stored in the submodules of the upper and those of the lower arms.

The p.u. mathematical model can be obtained from [37], [41] by considering the same base for the power and energy quantities and the auxiliary variables defined in (3), (4). Hence, the converter energy difference is given by:

$$\dot{W}_\Delta = -e_{sum,d}i_{s,d} - e_{sum,q}i_{s,q} + e_{dif,d}i_{cir,d} + e_{dif,q}i_{cir,q} \tag{17}$$

and the converter total energy is given by:

$$\begin{aligned}\dot{W} \quad = &-\tfrac{1}{2}e_{dif,d}i_{s,d} - \tfrac{1}{2}e_{dif,q}i_{s,q} + 2e_{sum,d}i_{cir,d} + \\ &2e_{sum,q}i_{cir,q} + 4e_{sum,0}i_{cir,0}.\end{aligned} \tag{18}$$

The energy difference and the converter energy are obtained from the submodules voltage measurements that are readily available to the capacitor balancing algorithm. We refer the reader to [42] for details.

E. MMC Operation in GFM Mode

In this subsection, the mathematical model of the interaction of the MMC operating in GFM mode with the main electric grid is derived. The connection of the MMC converter station to the electric grid is shown in Fig. 3.

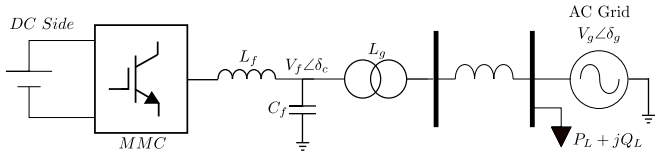

Fig. 3: Model of an MMC station operating in GFM converter mode connected to the electric grid.

The electric grid is modeled as an equivalent synchronous generator and an equivalent load [1], [43]. The generator is represented by the classical machine model that considers the generator as a complex voltage source ($\hat{V}_g = V_g\angle\delta_g$) behind a reactance. Two key assumptions of this model are that the rotor angle coincides with the phase angle δ_g of the voltage source and that the magnitude of $|\hat{V}_g|$ is constant.

The dynamic equations of the electric grid model are given by:

$$\begin{cases}\dot{\delta}_g = \omega_g \\ \dot{\omega}_g = \frac{1}{M_g}\Big(P_{m,g} + P_{e,c} - P_L\Big)\end{cases} \tag{19}$$

where ω_g is the grid frequency deviation from the synchronous frequency, M_g is the inertia constant of the equivalent generator and $P_{m,g}$, $P_{e,c}$, and P_L are respectively the mechanical power applied to the equivalent generator, the electrical power received by the equivalent generator shown below, and the equivalent load of the grid.

When the VSM GFM operation is considered, the converter displays the same dynamic behavior as a synchronous machine. Therefore, the converter is considered as a complex voltage source behind a reactance ($\hat{V}_f = V_f\angle\delta_c$) and the converter dynamics is written as the classic machine model as follows:

$$\begin{cases}\dot{\delta}_c = \omega_c \\ \dot{\omega}_c = \frac{1}{M_v}\Big[\bar{P}_c - K_c(\omega_c - \omega_g) - P_{e,c}\Big]\end{cases} \tag{20}$$

where ω_c is the deviation of the converter frequency from the synchronous frequency, M_v is the virtual inertia constant, K_c is the virtual damping coefficient, $\overline{P}_c$ is the active power reference that comes from a higher level controller not discussed in this paper, and $P_{e,c}$ is the active power delivered by the converter, calculated by:

$$P_{e,c} = \frac{|V_g||V_f|}{X_{eq}}\sin(\delta_c - \delta_g) \tag{21}$$

where $|V_f|$ is the magnitude of the voltage generated by the converter, δ_c is the converter output voltage phase angle and X_{eq} is the equivalent reactance obtained by adding up the transformer and the line reactances shown in Fig. 3.

The active power calculated by (21) is related to the model presented in subsections II-A through II-D by the following expression (in p.u. values):

$$P_{e,c} = v_{f,d}i_{s,d} + v_{f,q}i_{s,q} \tag{22}$$

with

$$|V_f| = \sqrt{v_{f,d}^2 + v_{f,q}^2}. \tag{23}$$

By defining:

$$\delta = \delta_c - \delta_g, \tag{24}$$

$$\tilde{\omega} = \omega_c - \omega_g, \tag{25}$$

the equivalent Single Machine Infinity Bus model that describes the interaction between the GFM MMC station and the electric grid is finally obtained subtracting (19) from (20) (see [1], [43] for details) as:

$$\begin{cases}\dot{\delta} = \tilde{\omega} \\ \dot{\tilde{\omega}} = -K_c'\tilde{\omega} + \frac{1}{M_{eq}}\Big(P_{mec} - P_{max}\sin\delta - P_L'\Big)\end{cases} \tag{26}$$

where M_{eq}, P_{mec}, P_{max}, K_c' and P_L' are defined by:

$$M_{eq} = \frac{M_vM_g}{M_v + M_g},\ P_{mec} = \frac{M_g\bar{P}_c - M_vP_{m,g}}{M_v + M_g} \tag{27}$$

$$P_{max} = \frac{|V_g||V_f|}{X_{eq}},\ K_c' = \frac{M_gK_c}{M_v + M_g},\ P_L' = \frac{-M_vP_L}{M_v + M_g}. \tag{28}$$

The equilibrium point of the equivalent AC grid modeled by (19) is a function of the external parameter represented by the load P_L. The grid frequency will respond to the instantaneous balance of produced and consumed power. Higher level controllers, here represented by $P_{m,g}$, will respond to this unbalance in a time frame of $10s$. For this reason, throughout this paper, it is assumed that $P_{m,g}$ is constant while the disturbance takes place. In a traditional grid-following

converter, the MMC-HVDC station would simply follow the new frequency of the grid, injecting a constant power $P_{e,c}$ into the AC grid, with $\omega_c \equiv \omega_g$.

However, GFM converters as in (20) have a different frequency ω_c, that will physically create a power variation in response to a grid frequency variation ω_g (and in consequence δ_g), represented by (21). This instantaneous variation on the provided power, will in its turn create a dynamic change in the converter frequency ω_c following (20). This behavior is known as frequency support and takes different forms with respect to different parameters and control objectives. For example, one can remark that the equivalent model (26) includes a modified inertia constant M_{eq} that takes into account the virtual inertia M_v brought by the GFM converter. This frequency support is of capital importance as discussed in the introduction, and allows the design of higher-level controllers for the converter, such as fast-frequency and primary frequency supports. These higher level controllers are out of the scope of the present paper, that focus on developing a stable control scheme that allows this frequency support.

In addition to the dynamic response presented above, it is important to remark that a change in the converter frequency ω_c will result in changes in $i_{s,dq}$ output current according to (22). These dynamic responses will in their turn create even others, as modeled in subsection II-F.

F. Modeling of the MMC Controlled as a GFM Converter

The purpose of this section is to consolidate the modeling of the MMC converter station controlled as a VSM. Let us define the state as

$$x = [x_s^T \;\; x_v^T \;\; x_{cir}^T \;\; x_W^T \;\; x_\omega^T]^T \tag{29}$$

where

$$x_s = [i_{s,d} \;\; i_{s,q}]^T, \quad x_v = [v_{f,d} \;\; v_{f,q}]^T \tag{30}$$

$$x_{cir} = [i_{cir,d} \;\; i_{cir,q} \;\; i_{cir,0}]^T, \quad x_W = [W_\Delta \;\; W]^T \tag{31}$$

$$x_\omega = [\delta \;\; \tilde{\omega}]^T \tag{32}$$

and the input vector is:

$$u = [e_{dif,d} \;\; e_{dif,q} \;\; e_{sum,d} \;\; e_{sum,q} \;\; e_{sum,0}]^T. \tag{33}$$

Moreover, let us define the exogenous input vector as:

$$u_e = [i_{g,d} \;\; i_{g,q} \;\; \delta_g \;\; \omega_g \;\; P_{m,g} \; P_L]^T. \tag{34}$$

Part of the exogenous input vector is composed of standard measures, namely the currents flowing into the PCC, i.e., $i_{g,d}, i_{g,q}$, and the grid frequency deviation ω_g.

Then, the full system model is

$$\begin{cases} \dot{i}_{s,d} = -\frac{\omega_b r_{eq}}{l_{eq}} i_{s,d} + \omega\omega_b i_{s,q} + \frac{\omega_b}{l_{eq}} e_{dif,d} + \frac{2\omega_b}{l_{eq}} v_{f,d} \\ \dot{i}_{s,q} = -\omega\omega_b i_{s,d} - \frac{\omega_b r_{eq}}{l_{eq}} i_{s,q} + \frac{\omega_b}{l_{eq}} e_{dif,q} + \frac{2\omega_b}{l_{eq}} v_{f,q} \\ \dot{v}_{f,d} = \frac{\omega_b}{c_f}(i_{g,d} - i_{s,d}) + \omega\omega_b v_{f,q} \\ \dot{v}_{f,q} = \frac{\omega_b}{c_f}(i_{g,q} - i_{s,q}) - \omega\omega_b v_{f,d} \\ \dot{i}_{cir,d} = -\frac{\omega_b r}{l} i_{cir,d} + \omega\omega_b i_{cir,q} - \frac{\omega_b}{l} e_{sum,d} \\ \dot{i}_{cir,q} = -\omega\omega_b i_{cir,d} - \frac{\omega_b r}{l} i_{cir,q} - \frac{\omega_b}{l} e_{sum,q} \\ \dot{i}_{cir,0} = -\frac{\omega_b r}{l} i_{cir,0} - \frac{\omega_b}{l} e_{sum,0} + \frac{\omega_b}{l} v_{dc} \\ \dot{W}_\Delta = -e_{sum,d} i_{s,d} - e_{sum,q} i_{s,q} + e_{dif,d} i_{cir,d} + e_{dif,q} i_{cir,q} \\ \dot{W} = -\frac{1}{2} e_{dif,d} i_{s,d} - \frac{1}{2} e_{dif,q} i_{s,q} + 2e_{sum,d} i_{cir,d} \\ \qquad +2e_{sum,q} i_{cir,q} + 4e_{sum,0} i_{cir,0} \\ \dot{\delta} = \tilde{\omega} \\ \dot{\tilde{\omega}} = -K'_c \tilde{\omega} + \frac{1}{M_{eq}} \left(P_{mec} - P_{max} sin\delta - P'_L \right) \end{cases} \tag{35}$$

which can be summarized as follows:

$$\dot{x}(t) = f(x(t)) + g(x(t))u(t) + h(u_e(t)) \tag{36}$$

where f, g and h are obtained from (9), (10), (11), (12), (14), (15), (16), (17), (18) and (26). More in detail, the function f contains the linear terms and the sine, while g contains constant terms and the state variables for the bilinear terms in the energy equations.

The state $x \in \mathbb{R}^{11}$ is composed by the output and circulating currents, the output voltage, the converter energy and the GFM interaction with the electric grid. The state variables x_s are the output currents in dq frame, x_v are the components of the output voltage in the dq frame, x_{cir} are the circulating currents in the $dq0$ frame, x_W are the energy difference and the total energy of the converter and x_ω are the variables associated with the GFM operation.

As seen in [37], considering the arm voltages as control inputs embeds an additional complexity to the design of the control inputs as two control inputs would be present in the output and circulating currents models. Hence, by considering the input vector $u \in \mathbb{R}^5$ in (33), composed by the auxiliary inputs defined in (3) and (4), the control design is simplified. Then, after the control laws u are obtained, the arm voltages $v_{u,dq0}$ and $v_{l,dq0}$ are calculated by:

$$v_{u,j} = e_{sum,j} + \frac{1}{2} e_{dif,j} \tag{37}$$

$$v_{l,j} = e_{sum,j} - \frac{1}{2} e_{dif,j} \tag{38}$$

where the subscript j denotes the d, q or 0 components.

The exogenous input vector $u_e \in \mathbb{R}^6$ is composed of the grid currents $i_{g,dq}$, the grid phase angle δ_g, the grid's frequency ω_g, the mechanical power applied to the equivalent synchronous generator modeling the equivalent electric grid and P_L is the system load.

III. Controllers for the MMC in GFM Mode

The objective of this work is to develop a nonlinear control strategy that enables the MMC to operate in the GFM converter mode. The control system is designed such that it is able

to track the reference values for the output voltage $\overline{v}_{f,d}$ and $\overline{v}_{f,q}$, total converter energy $\overline{W}$, and energy difference $\overline{W}_\Delta$, and that the active power exchanged with the electric grid $P_{c,e}$ follows the classical machine model. The design of the proposed control strategy relies upon feedback linearization [44] and dynamic feedback linearization [45]–[47]. The use of nonlinear tools applied to GFM operation of the MMC is part of the contribution of this work.

The controller is based on a Lyapunov function that is used to design the desired trajectories and the control inputs such that the stability of the converter station is assured. To this purpose, we define the following trajectories $i^*_{s,d}$, $i^*_{s,q}$, $i^*_{cir,d}$ and $i^*_{cir,0}$ for the dynamics $i_{s,d}$, $i_{s,q}$, $i_{cir,d}$ and $i_{cir,0}$ as:

$$i^*_{s,d} = i_{g,d} + \frac{c_f}{\omega_b}\left[\omega\omega_b v_{f,q} + K_3(v_{f,d} - \overline{v}_{f,d}) + K_3^\alpha \alpha_3\right] \quad (39)$$

$$i^*_{s,q} = i_{g,q} + \frac{c_f}{\omega_b}\left[-\omega\omega_b v_{f,d} + K_4(v_{f,q} - \overline{v}_{f,q}) + K_4^\alpha \alpha_4\right] \quad (40)$$

$$i^*_{cir,d} = -\frac{K_8(W_\Delta - \overline{W}_\Delta) + K_8^\alpha \alpha_8}{r'_{eq} i^*_{s,d} + \omega l'_{eq} i^*_{s,q} - 2v_{f,d} + (v_{f,d} - \overline{v}_{f,d})\frac{l_{eq}}{c_f}} \quad (41)$$

$$i^*_{cir,0} = \int \frac{1}{4v_{dc} - 8r i^*_{cir,0}}[\Psi_9 - K_9 \dot{W} - K_9^\alpha (W - \overline{W})]dt \quad (42)$$

where K_i and K_i^α, $i = \{3, 4, 8, 9\}$ are the controller gains and:

$$\begin{aligned}\Psi_9 =& r_{eq} i^*_{s,d} \dot{i}^*_{s,d} + r_{eq} i^*_{s,q} \dot{i}^*_{s,q} - v_{f,d} \dot{i}^*_{s,d} - \dot{v}_{f,d} i^*_{s,d} \\ & - v_{f,q} \dot{i}^*_{s,q} - \dot{v}_{f,q} i^*_{s,q} + 4r i^*_{cir,d} \dot{i}^*_{cir,d}\end{aligned} \quad (43)$$

and l'_{eq} and r'_{eq} given by:

$$l'_{eq} = l - l_{eq}, \quad r'_{eq} = r + r_{eq} \quad (44)$$

It is noteworthy to highlight that the denominators of (41) and (42) are always different from zero, by physical reasons. These terms represent the nonzero voltage drop when current flows through a resistor.

To ensure zero tracking error in steady-state, integral terms α_3, α_4 and α_8 are defined as:

$$\dot{\alpha}_3 = v_{f,d} - \overline{v}_{f,d}, \quad \dot{\alpha}_4 = v_{f,q} - \overline{v}_{f,q} \quad (45)$$

$$\dot{\alpha}_8 = W_\Delta - \overline{W}_\Delta \quad (46)$$

To steer the dynamics $i_{s,d}$, $i_{s,q}$, $i_{cir,d}$ and $i_{cir,0}$ to their respective desired trajectories (39), (40), (41) and (42), and to steer $i_{cir,q}$ to its desired set-point $\bar{i}_{cir,q}$ (that is chosen as zero to minimize power losses [37]), the following control inputs are introduced:

$$\begin{aligned}e_{dif,d} =& r_{eq} i_{s,d} - l_{eq}\omega i_{s,q} - 2v_{f,d} + (v_{f,d} - \overline{v}_{f,d})\frac{l_{eq}}{c_f} \\ & + \frac{l_{eq}}{\omega_b}\left[\dot{i}^*_{s,d} - K_1(i_{s,d} - i^*_{s,d}) - K_1^\alpha \alpha_1\right]\end{aligned} \quad (47)$$

$$\begin{aligned}e_{dif,q} =& r_{eq} i_{s,q} + l_{eq}\omega i_{s,d} - 2v_{f,q} - (v_{f,q} + \overline{v}_{f,q})\frac{l_{eq}}{c_f} \\ & + \frac{l_{eq}}{\omega_b}\left[\dot{i}^*_{s,q} - K_2(i_{s,q} - i^*_{s,q}) - K_2^\alpha \alpha_2\right]\end{aligned} \quad (48)$$

$$\begin{aligned}e_{sum,d} =& - r i_{cir,d} + l\omega i_{cir,q} \\ & - \frac{l}{\omega_b}\dot{i}^*_{cir,d} + K_5(i_{cir,d} - i^*_{cir,d}) + K_5^\alpha \alpha_5,\end{aligned} \quad (49)$$

$$e_{sum,q} = -l\omega i_{cir,d} - r i_{cir,q} + K_6(i_{cir,q} - \bar{i}_{cir,q}) + K_6^\alpha \alpha_6, \quad (50)$$

$$e_{sum,0} = -r i_{cir,0} + v_{dc} - \frac{l}{\omega_b}\dot{i}^*_{cir,0} + K_7(i_{cir,0} - i^*_{cir,0}) + K_7^\alpha \alpha_7. \quad (51)$$

and the integral terms to ensure zero tracking error in steady-state are defined as:

$$\dot{\alpha}_1 = i_{s,d} - i^*_{s,d} \quad \dot{\alpha}_2 = i_{s,q} - i^*_{s,q}, \quad (52)$$

$$\dot{\alpha}_5 = i_{cir,d} - i^*_{cir,d}, \quad \dot{\alpha}_6 = i_{cir,q} - \bar{i}_{cir,q}, \quad \dot{\alpha}_7 = i_{cir,0} - i^*_{cir,0}. \quad (53)$$

The gains K_i and K_i^α, $i = \{1, ..., 9\}$ are positive real numbers and are the tuning parameters of the proposed controller. Their values can be obtained by pole placement of a second order system, specifying the desired settling time and damping as in [48].

The controllers here introduced ensure the asymptotic stability of an extended system considering also the control dynamics, as demonstrated in the following Section.

IV. Stability Analysis

To evaluate the stability of the MMC converter station modeled by (36) in closed loop following the trajectories and control inputs presented in this section, the following extended state χ and its equilibrium point χ_e are defined:

$$\chi = [\chi_s^T \ \chi_v^T \ \chi_{cir}^T \ \chi_W^T \ \chi_\omega^T]^T \quad (54)$$

$$\chi_e = [\chi_{s,e}^T \ \chi_{v,e}^T \ \chi_{cir,e}^T \ \chi_{W,e}^T \ \chi_{\omega,e}^T]^T \quad (55)$$

where

$$\chi_s = [i_{s,d} \ \alpha_1 \ i_{s,q} \ \alpha_2]^T; \ \chi_{s,e} = [i^*_{s,d} \ 0 \ i^*_{s,q} \ 0]^T; \quad (56)$$

$$\chi_v = [v_{f,d} \ \alpha_3 \ v_{f,q} \ \alpha_4]^T; \ \chi_{v,e} = [\overline{v}_{f,d} \ 0 \ \overline{v}_{f,q} \ 0]^T; \quad (57)$$

$$\begin{aligned}&\chi_{cir} = [i_{cir,d} \ \alpha_5 \ i_{cir,q} \ \alpha_6 \ i_{cir,0} \ \alpha_7]^T; \\ &\chi_{cir,e} = [i^*_{cir,d} \ 0 \ \bar{i}_{cir,q} \ 0 \ i^*_{cir,0} \ 0]^T;\end{aligned} \quad (58)$$

$$\chi_W = [W_\Delta \ \alpha_8 \ W \ \dot{W}]^T; \ \chi_{W,e} = [\overline{W}_\Delta \ 0 \ \overline{W} \ 0]^T; \quad (59)$$

$$\chi_\omega = [\delta \ \ \tilde{\omega}]^T; \ \chi_{\omega,e} = [\delta_s \ \ 0]^T \quad (60)$$

with

$$\delta_s = \arcsin\left(\frac{P'_L - P_{mec}}{P_{max}}\right). \quad (61)$$

Moreover, let us consider the following conditions:

$$\begin{aligned}r'_{eq} i^*_{s,d} + \omega l'_{eq} i^*_{s,q} - 2v_{f,d} + (v_{f,d} - \overline{v}_{f,d})\frac{l_{eq}}{c_f} \neq 0 \\ 4v_{dc} - 8r i^*_{cir,0} \neq 0\end{aligned} \quad (62)$$

and the physical limitations of the control inputs:

$$e_{dif,j} \ \in \left[-\frac{v_{dc}}{2}, \ \frac{v_{dc}}{2}\right], \ j = d, q \quad (63)$$

$$e_{sum,j} \ \in \left[-\frac{v_{dc}}{2}, \ \frac{v_{dc}}{2}\right], \ j = d, q, 0. \quad (64)$$

A key assumption made is that the power system has enough power reserves available. This condition can be translated into a set Ω of possible operating points $(\delta_g, \omega_g, P_{m,g}, P_L, \delta_c, \omega, \overline{P})$, where (19), (20) and (26) have a physically feasible stable equilibrium point and the conditions (62)-(64) are met. We also assume that the set $\overline{\Omega}$ of all possible reference values of $\bar{i}_{cir,q}$, $\overline{v}_{f,d}$, $\overline{v}_{f,q}$, $\overline{W}_\Delta$ and $\overline{W}$ is nonempty when $(\delta_g, \omega_g, P_{m,g}, P_L, \delta_c, \omega, \overline{P}) \in \Omega$.

Then, we state the following stability result.

Theorem 1. Let us consider the designed trajectories $i^*_{s,d}$, $i^*_{s,q}$, $i^*_{cir,d}$ and $i^*_{cir,0}$ in (39), (40), (41) and (42), respectively, and the control inputs $e_{dif,d}$, $e_{dif,q}$, $e_{sum,d}$, $e_{sum,q}$ and $e_{sum,0}$ given by (47), (48), (49), (50) and (51). For any given $(\delta_g, \omega_g, P_{m,g}, P_L, \delta_c, \omega, \overline{P}) \in \Omega$ and any given $\{\bar{i}_{cir,q}, \overline{v}_{f,d}, \overline{v}_{f,q}, \overline{W}_\Delta\} \in \overline{\Omega}$ such that the conditions (62)-(64) are met, the MMC introduced in (36) and modeled in closed loop by the extended state χ in (54) is asymptotically stable with respect to the equilibrium χ_e in (55).

Proof. To prove asymptotic stability of the model in (36), we refer to the state χ in (54) with respect to its equilibrium χ_e in (55). In the sequel, we refer to [44] for the definition of Lyapunov functions, Lyapunov stability analysis and backstepping control design. We refer to [45] for the definition of dynamic feedback linearization.

To prove stability, we target a Lyapunov function $\mathcal{V}_\chi$ as a composition of Lyapunov defined as:

$$\mathcal{V}_\chi = \mathcal{V}_s + \mathcal{V}_v + \mathcal{V}_{cir} + \mathcal{V}_W + \mathcal{V}_\omega > 0. \tag{65}$$

Let us start with the voltages $v_{f,d}$ and $v_{f,q}$ with respect to the desired equilibria $\overline{v}_{f,d}$ and $\overline{v}_{f,q}$. Targeting to use backstepping, we define the candidate Lyapunov functions $\mathcal{V}_3$ and $\mathcal{V}_4$ as

$$\mathcal{V}_3 = \frac{1}{2}(v_{f,d} - \overline{v}_{f,d})^2 + \frac{K_3^\alpha}{2}\alpha_3^2 > 0, \tag{66}$$

$$\mathcal{V}_4 = \frac{1}{2}(v_{f,q} - \overline{v}_{f,q})^2 + \frac{K_4^\alpha}{2}\alpha_4^2 > 0. \tag{67}$$

Then, by computing the time derivative of $\dot{\mathcal{V}}_3$ according to (11) and the definition of the backstepping change of coordinates as $z = i_{s,d} - i^*_{s,d}$, it results

$$\begin{aligned}\dot{\mathcal{V}}_3 =&(v_{f,d} - \overline{v}_{f,d})\left(\frac{\omega_b}{c_f}(i_{g,d} - i_{s,d}) + \omega\omega_b v_{f,q} + K_3^\alpha\alpha_3\right)\\ =&(v_{f,d} - \overline{v}_{f,d})\left(\frac{\omega_b}{c_f}(i_{g,d} - i^*_{s,d}) + \omega\omega_b v_{f,q} + K_3^\alpha\alpha_3\right)\\ &+ (v_{f,d} - \overline{v}_{f,d})\frac{\omega_b}{c_f}\left(i^*_{s,d} - i_{s,d}\right).\end{aligned} \tag{68}$$

Then, by substitution of $i^*_{s,d}$ as in (39), it results

$$\dot{\mathcal{V}}_3 = -K_3(v_{f,d} - \overline{v}_{f,d})^2 + (v_{f,d} - \overline{v}_{f,d})\frac{\omega_b}{c_f}\left(i^*_{s,d} - i_{s,d}\right).$$

To the goal to iterate the backstepping procedure, we define $\mathcal{V}_1$ as

$$\mathcal{V}_1 = \frac{1}{2}(i_{s,d} - i^*_{s,d})^2 + \frac{K_1^\alpha}{2}\alpha_1^2 > 0 \tag{69}$$

and by computing the time derivative of $\mathcal{V}_1 + \mathcal{V}_3$, i.e., $\dot{\mathcal{V}}_1 + \dot{\mathcal{V}}_3$, and considering the dynamics of $i_{s,d}$ in (9), it results

$$\begin{aligned}\dot{\mathcal{V}}_1 + \dot{\mathcal{V}}_3 =&(i_{s,d} - i^*_{s,d})\left(-\frac{\omega_b r_{eq}}{l_{eq}}i_{s,d} + \omega\omega_b i_{s,q} + \frac{2\omega_b}{l_{eq}}v_{f,d}\right)\\ &+(i_{s,d} - i^*_{s,d})\left(\frac{\omega_b}{l_{eq}}e_{dif,d} - \dot{i}^*_{s,d} + K_1^\alpha\alpha_1\right)\\ &+(i_{s,d} - i^*_{s,d})\left(-(v_{f,d} - \overline{v}_{f,d})\frac{\omega_b}{c_f}\right)\\ &-K_3(v_{f,d} - \overline{v}_{f,d})^2.\end{aligned}$$

Thus, by considering $e_{dif,d}$ in (47) it results a negative semi-definite time derivative, as Similar computations lead to consider $\mathcal{V}_4$ together to $\mathcal{V}_2$, with

$$\mathcal{V}_2 = \frac{1}{2}(i_{s,q} - i^*_{s,q})^2 + \frac{K_2^\alpha}{2}\alpha_2^2 > 0. \tag{70}$$

By considering similar computations for $i^*_{s,q}$ in (40) and $e_{dif,q}$ in (48), it results

$$\mathcal{V}_2 + \mathcal{V}_4 > 0 \tag{71}$$

and

$$\dot{\mathcal{V}}_2 + \dot{\mathcal{V}}_4 \leq 0. \tag{72}$$

Then, we define

$$\mathcal{V}_s + \mathcal{V}_v = \mathcal{V}_1 + \mathcal{V}_2 + \mathcal{V}_3 + \mathcal{V}_4 > 0 \tag{73}$$

such that

$$\dot{\mathcal{V}}_s + \dot{\mathcal{V}}_v = \dot{\mathcal{V}}_1 + \dot{\mathcal{V}}_2 + \dot{\mathcal{V}}_3 + \dot{\mathcal{V}}_4 \leq 0. \tag{74}$$

To the goal to prove asymptotic convergence of the dynamics, we first write the closed-loop equations. It results

$$\begin{aligned}\dot{i}_{s,d} =& \dot{i}^*_{s,d} + \frac{\omega_b}{c_f}(v_{f,d} - \overline{v}_{f,d}) - K_1^\alpha\alpha_1\\ &- K_1\left[i_{s,d} - i_{g,d} - c_f\omega v_{f,q} - \frac{c_f}{\omega_b}K_3^\alpha\alpha_3 - \frac{c_f}{\omega_b}K_3(v_{f,d} - \overline{v}_{f,d})\right]\end{aligned} \tag{75a}$$

$$\begin{aligned}\dot{i}_{s,q} =& \dot{i}^*_{s,q} + \frac{\omega_b}{c_f}(v_{f,q} - \overline{v}_{f,q}) - K_2^\alpha\alpha_2\\ &- K_2\left[i_{s,q} - i_{g,q} + c_f\omega v_{f,d} - \frac{c_f}{\omega_b}K_4^\alpha\alpha_4 - \frac{c_f}{\omega_b}K_4(v_{f,d} - \overline{v}_{f,d})\right]\end{aligned} \tag{75b}$$

$$\dot{\alpha}_1 = i_{s,d} - i_{g,d} + \frac{c_f}{\omega_b}\left[-\omega\omega_b v_{f,q} - K_3(v_{f,d} - \overline{v}_{f,d}) - K_3^\alpha\alpha_3\right] \tag{75c}$$

$$\dot{\alpha}_2 = i_{s,q} - i_{g,q} + \frac{c_f}{\omega_b}\left[\omega\omega_b v_{f,d} - K_4(v_{f,q} - \overline{v}_{f,q}) - K_4^\alpha\alpha_4\right] \tag{75d}$$

$$\dot{v}_{f,d} = \frac{\omega_b}{c_f}(i_{g,d} - i_{s,d}) + \omega\omega_b v_{f,q} \tag{75e}$$

$$\dot{v}_{f,q} = \frac{\omega_b}{c_f}(i_{g,q} - i_{s,q}) - \omega\omega_b v_{f,d} \tag{75f}$$

$$\dot{\alpha}_3 = v_{f,d} - \overline{v}_{f,d} \tag{75g}$$

$$\dot{\alpha}_4 = v_{f,q} - \overline{v}_{f,q}. \tag{75h}$$

By computing the equilibrium points, from (75g) and (75h) it results that the equilibrium for $v_{f,d}$ and $v_{f,q}$ are $\overline{v}_{f,d}$ and $\overline{v}_{f,q}$, respectively. By substituting those values in equations (75e) and (75f), it results that $i^{eq}_{s,d} = i_{g,d} + c_f\omega_b\overline{v}_{f,q}$ and

$i^{eq}_{s,q} = i_{g,q} - c_f \omega_b \overline{v}_{f,d}$, respectively. Then, from (75c) and (75d) simple computations lead to the results that the equilibrium for α_3 and α_4 is zero. By iterating the behaviors with (75a) and (75b), the equilibrium point for α_1 and α_2 are shown to be equal to zero as well. Therefore, by using Lasalle's Theorem, it is possible to prove that the subsystem composed by these dynamics converges to the maximal invariant set that is composed of the equilibrium equal to zero for the integral error terms. More details will be given in the following of the proof.

Before focusing on the convergence for the energy dynamics in (59), we need to remark that the design of the trajectories $i^*_{cir,d}$ and $i^*_{cir,0}$ that ensures the convergence of W_Δ and W to their respective reference values $\overline{W}_\Delta$ and $\overline{W}$ can not be made by the same backstepping-like procedure adopted until now. The trajectories $i^*_{cir,d}$ and $i^*_{cir,0}$ have to be designed according to time-scale separation principles, which allows to consider the slow dynamics of x_W when the fast dynamics of x_s and x_{cir} have already reached their reference trajectories. Therefore, when considering the circulating currents χ_{cir} in (58), we select the candidate Lyapunov function $\mathcal{V}_{cir}$, where

$$\mathcal{V}_{cir} = \mathcal{V}_5 + \mathcal{V}_6 + \mathcal{V}_7 > 0 \tag{76}$$

and defined as the sum of the following functions:

$$\mathcal{V}_5 = \frac{1}{2}(i_{cir,d} - i^*_{cir,d})^2 + \frac{K^\alpha_5}{5}\alpha_5^2 > 0 \tag{77}$$

$$\mathcal{V}_6 = \frac{1}{2}(i_{cir,q} - \bar{i}_{cir,q})^2 + \frac{K^\alpha_6}{6}\alpha_6^2 > 0 \tag{78}$$

$$\mathcal{V}_7 = \frac{1}{2}(i_{cir,0} - i^*_{cir,0})^2 + \frac{K^\alpha_7}{7}\alpha_7^2 > 0. \tag{79}$$

It is easy to verify that the control inputs in (49), (50) and (51) are designed such that:

$$\dot{\mathcal{V}}_5 = -K_5(i_{cir,d} - i^*_{cir,d})^2 \leq 0 \tag{80}$$

$$\dot{\mathcal{V}}_6 = -K_6(i_{cir,q} - \bar{i}_{cir,q})^2 \leq 0 \tag{81}$$

$$\dot{\mathcal{V}}_7 = -K_7(i_{cir,0} - i^*_{cir,0})^2 \leq 0. \tag{82}$$

Similarly to the previous case, we cannot prove asymptotic convergence just by considering the Lyapunov functions, as their time derivatives are negative semi-definite. However, by writing the closed loop dynamics, it results that the only equilibrium point for α_5, α_6 and α_7 is zero:

$$\dot{i}_{cir,d} = \dot{i}^*_{cir,d} - K_5(i_{cir,d} - i^*_{cir,d}) - K^\alpha_5\alpha_5 \tag{83a}$$

$$\dot{\alpha}_5 = i_{cir,d} - i^*_{cir,d} \tag{83b}$$

$$\dot{i}_{cir,q} = -K_6(i_{cir,q} - \bar{i}_{cir,q}) - K^\alpha_6\alpha_6 \tag{83c}$$

$$\dot{\alpha}_6 = i_{cir,q} - \bar{i}_{cir,q} \tag{83d}$$

$$\dot{i}_{cir,0} = \dot{i}^*_{cir,0} - K_7(i_{cir,0} - i^*_{cir,0}) - K^\alpha_7\alpha_7 \tag{83e}$$

$$\dot{\alpha}_7 = i_{cir,0} - i^*_{cir,0} \tag{83f}$$

From these properties, according to a proper choice of the control gains K_5, K_6, and K_7 such to ensure the multi-time scale behavior of circulating currents with respect to the energy variations, as it is natural also physically, it follows that it is possible to consider $i_{s,dq} = i^*_{s,dq}$, $i_{cir,d0} = i^*_{cir,d0}$ and $i_{cir,q} = \bar{i}_{cir,q}$ for the energy dynamics, which allows us to consider (17) and (18) as:

$$\dot{W}_\Delta = -e_{sum,d}i^*_{s,d} - e_{sum,q}i^*_{s,q} + e_{dif,d}i^*_{cir,d} + e_{dif,q}\bar{i}_{cir,q} \tag{84}$$

$$\begin{aligned}\dot{W} \quad &= -\tfrac{1}{2}e_{dif,d}i^*_{s,d} - \tfrac{1}{2}e_{dif,q}i^*_{s,q} + 2e_{sum,d}i^*_{cir,d} \\ &\quad + 2e_{sum,q}\bar{i}_{cir,q} + 4e_{sum,0}i^*_{cir,0}.\end{aligned} \tag{85}$$

We recall that the references $i^*_{cir,d}$ and $i^*_{cir,0}$ are still degrees of freedom for controlling (84) and (85), respectively. The selection of those references is operated by using feedback linearisation (see [44]) for $i^*_{cir,d}$ and dynamic feedback linearization (see [45], [49]) for $i^*_{cir,0}$. To prove the proper selection of $i^*_{cir,d}$ as in (41), we start defining $\mathcal{V}_8$ as

$$\mathcal{V}_8 = \frac{1}{2}(W_\Delta - \overline{W}_\Delta)^2 + \frac{K^\alpha_8}{2}\alpha_8^2 > 0. \tag{86}$$

By simple computation, it is easy to obtain that the trajectory (41) is designed by feedback linearization such that the time derivative $\dot{\mathcal{V}}_8$ is negative semi-definite, i.e.,

$$\dot{\mathcal{V}}_8 = -K_8(W_\Delta - \overline{W}_\Delta)^2 \leq 0. \tag{87}$$

Again, we show that the only possible equilibrium for this subsystem is the one where the equilibrium for α_8 is equal to zero:

$$\dot{W}_\Delta = -K_8(W_\Delta - \overline{W}_\Delta) - K^\alpha_8\alpha_8, \tag{88a}$$

$$\dot{\alpha}_8 = W_\Delta - \overline{W}_\Delta. \tag{88b}$$

When manipulating the model in (85) by substituting the equilibrium values of the control input vector u, the desired trajectory $i^*_{cir,0}$ appears as a squared term. As a consequence, it is not possible to directly use feedback linearization to design the trajectory. The proposed solution to design $i^*_{cir,0}$, thus leading to the value in (42), is the application of dynamic feedback linearization [45], considering its time derivative $\dot{i}^*_{cir,0}$ as a virtual input. Hence, by taking the second time derivative of W, we obtain:

$$\begin{aligned}\ddot{W} = &- r_{eq}i^*_{v,d}\dot{i}^*_{v,d} - r_{eq}i^*_{v,q}\dot{i}^*_{v,q} + v_{f,d}\dot{i}^*_{v,d} + \dot{v}_{f,d}i^*_{v,d} \\ &+ v_{f,q}\dot{i}^*_{v,q} + \dot{v}_{f,q}i^*_{v,q} - 4ri^*_{circ,d}\dot{i}^*_{circ,d} \\ &+ \left[4v_{dc} - 8ri^*_{circ,0}\right]\dot{i}^*_{circ,0}.\end{aligned} \tag{89}$$

From (89), one can note that the trajectory (42) is designed such that the converter energy dynamics subsystem, extended with the second time derivative of the energy, results in a stable linear system. Indeed, by the choice in (42) it results that:

$$\begin{bmatrix}\dot{W} \\ \ddot{W}\end{bmatrix} = A\begin{bmatrix}W - \overline{W} \\ \dot{W}\end{bmatrix},\ A = \begin{bmatrix}0 & 1 \\ -K^\alpha_9 & -K_9\end{bmatrix}. \tag{90}$$

When $K_9, K^\alpha_9 > 0$, matrix A is Hurwitz and, therefore, the system is stable. Consequently, due to the converse Lyapunov theorems, if the system is stable then it is possible to obtain a Lyapunov function $\mathcal{V}_9$ such that:

$$\mathcal{V}_9 > 0, \quad \dot{\mathcal{V}}_9 < 0. \tag{91}$$

Therefore, there exists a Lyapunov function $\mathcal{V}_W$ in the form

$$\mathcal{V}_W = \mathcal{V}_8 + \mathcal{V}_9 > 0 \tag{92}$$

that ensures exponential convergence of χ_W to its equilibrium point.

The last step of the proof is to investigate the convergence of the state variables that compose the dynamics χ_ω in (60). To this purpose, similarly to [43], the following Lyapunov function based on the energy function of the synchronous machine is proposed:

$$\mathcal{V}_\omega(\delta,\tilde{\omega}) = \frac{1}{2}M_{eq}\tilde{\omega}^2 + \int_{\delta_s}^{\delta}[P_{max}\sin\delta - P_{mec} + P'_L]d\delta > 0 \tag{93}$$

where δ_s in (61) is the stable equilibrium point obtained from the power balance of the system given by (26), since

$$\sin(\delta_s) = \left(\frac{P'_L - P_{mec}}{P_{max}}\right).$$

Then, it is possible to rewrite (93) as

$$\mathcal{V}_\omega(\delta,\tilde{\omega}) = \frac{1}{2}M_{eq}\tilde{\omega}^2 + P_{max}\int_{\delta_s}^{\delta}[\sin\delta - \sin\delta_s]d\delta > 0.$$

We stress that the integral term in $\mathcal{V}_\omega$ is positive if the following condition is satisfied:

$$\cos(\delta_s) - \cos(\delta) - \sin(\delta_s)(\delta_s - \delta) > 0. \tag{94}$$

From Fig. 4, we verify that there exist conditions satisfying (94), especially close to the origin. Then (93) is verified to be positive definite for some δ.

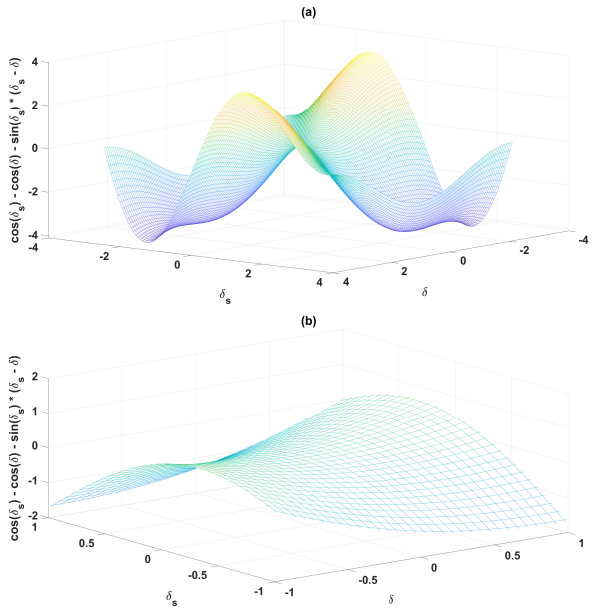

Fig. 4: a) The plot of the function in (94). b) A zoom around the origin.

Considering (26) and (93), the time derivative $\dot{\mathcal{V}}_\omega$ results

$$\dot{\mathcal{V}}_\omega = -K'_c\tilde{\omega}^2 \leq 0. \tag{95}$$

The time derivative $\dot{\mathcal{V}}_\omega$ is negative semi-definite, so no stability conditions can be ensured directly from (95) only. However, by an analysis of the system (26) we remark that the only possible equilibrium is $\chi_{\omega,e} = [\delta_s \;\; 0]^T$ in (60), with δ_s in (61).

To show asymptotic stability of the whole system χ, we remark that the composition of candidate Lyapunov functions $\mathcal{V}_\chi$ in (65) has a negative semi-definite time derivative, i.e., $\dot{\mathcal{V}}_\chi \leq 0$, according to the analysis of (74), (80), (81), (82), (87), (91) and (95):

$$\dot{\mathcal{V}}_\chi = \dot{\mathcal{V}}_s + \dot{\mathcal{V}}_v + \dot{\mathcal{V}}_{cir} + \dot{\mathcal{V}}_W + \dot{\mathcal{V}}_\omega \leq 0. \tag{96}$$

Hence, $\mathcal{V}_\chi$ and its time derivative $\dot{\mathcal{V}}_\chi$ in (96) meet the conditions for the application of Lasalle's theorem [44] for asymptotic stability. Let us consider the set E representing the points where the Lyapunov function is not decreasing. Then, let us consider the largest invariant set $\bar{E}$ in E. By the previous considerations for each subsystem, it results that this set contains a unique point, which is:

$$\bar{E} = \{\chi_e\}. \tag{97}$$

Therefore, applying LaSalle's theorem to the Lyapunov function $\mathcal{V}_\chi > 0$ in (65) and its negative semi-definite time derivative $\dot{\mathcal{V}}_\chi$ in (96), asymptotic stability of the equilibrium point can be established. This concludes the proof. ■

Remark. To improve clarity on the asymptotic stability property of the subsystem (26), we show its phase portrait in Fig. 5. It shows convergence around the equilibrium point (1,0).

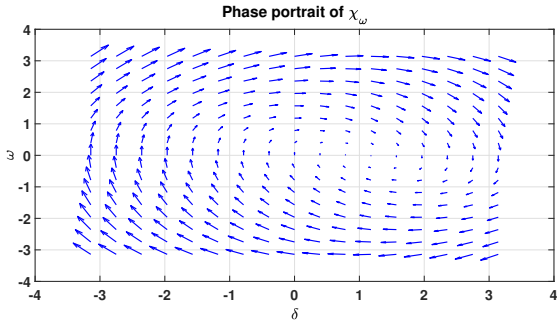

Fig. 5: The phase portrait of χ_ω with value $P_{max} = 1$ GW.

V. Simulation Results

In this work, we develop a control strategy compatible with VSM-GFM operation for an MMC based on nonlinear techniques. The control targets for an MMC operating as a GFM converter are to regulate the voltage phasor magnitude and the energy stored in the converter. When operating as a VSM, the voltage phasor's angle is obtained by a swing equation to mimic the behavior of the power output of a synchronous generator.

To validate the proposed controller, the model shown in Fig. 3 is implemented in Matlab/Simscape Electrical. The parameters considered for the MMC are shown in Table I and the parameters of the grid equivalent are given in Table II. For comparison purposes, a linear PI controller is also implemented in the test system. This section is divided in three subsections to validate the behavior of the closed loop system in three situations:

- Subsection V-A shows the results for the active power tracking when the MMC is subjected to a series of step changes in its active power reference value $\overline{P}_c$;
- Subsection V-B shows the results for the control system energy tracking when the MMC it is subjected to a series of step changes in its energy reference value $\overline{W}$;
- Subsection V-C shows the results for a situation where the MMC participates in the frequency support by contributing with virtual inertia to the system.

TABLE I: Parameters of the MMC controlled as a VSM

MMC Parameters				
S	V_f (L-L)	$\overline{W}$	v_{dc}	ω_c
1000 MVA	320 kV	25.8 MJ	640 kV	377 rad/s
N_{SM}	C_{SM}	C_{eq}	r	l
400	8.4 mF	21 μF	0.005 p.u.	0.1473 p.u.
r_f	l_f	c_f	r_g	l_g
0.01 p.u.	0.05 p.u.	0.193 p.u.	0.01 p.u.	0.05 p.u.
VSM Parameters				
M_c	3 s	K_c	320	

TABLE II: Parameters of the equivalent AC grid

Equivalent Grid Parameters				
S_{eq}	droop	Time Constant	M_g	P_L
3000 MW	3 %	5 s	2 s	2000 MW

A. Active Power Reference Tracking

One of the main operational requirements of an HVDC transmission system is to deliver active power at its dispatched value given by the power system operator. Hence, to validate the power reference tracking using the proposed controller, a sequence of steps is applied to the converter power reference $\overline{P}_c$ aiming to evaluate the closed loop system's response.

The active power response for a sequence of step changes in its reference value is shown in Fig. 6. The MMC controlled as a VSM-GFM converter with the proposed nonlinear (NL) controller is able to track the active power reference with accuracy. We point that the settling time is in the order of 1 s since the converter is mimicking the behavior of a SG when for GFL converter control strategies it is possible to track active power changes with settling times in the order of 1 ms. By exhibiting the behavior imposed by the proposed NL controller, the converter station does not change its active power output nearly instantaneously. Instead, the slower change in active power output emulates the physical inertia of the rotors of traditional SGs.

The same sequence of step changes in active power reference are also applied to the test system with the MMC station equipped with a PI controller. From Fig. 6, we note that the PI also tracks the active power reference with similar performance to the NL controller. To enable a closer comparison of the responses, Fig. 6 also shows a zoom of the first step change from 4.5 to 7 s.

The converter frequency is shown in Fig. 7. As a consequence of the shown active power responses, the NL and the PI controller resulted in a similar converter frequency. To compare closely both responses, a zoom corresponding to the first step change of the active power response is shown from 4.5 to 7 s. Since the phase angle of the converter is the integral of its frequency, the active power response shown in Fig. 6 is coherent with this result.

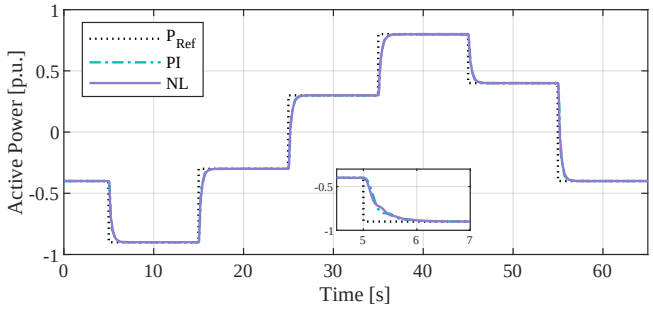

Fig. 6: Active power response subjected to a sequence of reference step changes.

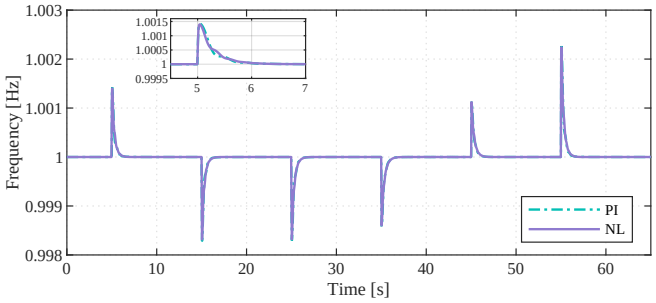

Fig. 7: Converter frequency response when the active power is subjected to a sequence of reference step changes.

However, despite presenting a similar performance for tracking the active power reference and for the converter frequency, these transient responses have a very different impact into the other variables of the system. As shown by (36), the MMC station state variables are dependent on one another, and therefore, a change in active power will affect the other state variables.

In GFM converters the change in frequency results in a disturbance in the values of currents and voltages in the $dq0$ frame given that the Park transformation is a function of the converter phase angle [50], differently from GFL converters where the converter frequency follows the grid's frequency. Therefore, the changes presented in Fig. 7 result in a disturbance in the magnitude of the terminal voltage $|V_f|$, as seen in Fig. 8.

The proposed NL controller is able to reject the disturbance caused by the frequency variation resulting from equipping the MMC station with GFM converter capabilities. Furthermore, we can see that the NL controller can perform a faster disturbance rejection than the PI controller. Moreover, the NL controller keeps the voltage level within a ± 0.7 % range from its reference value of 1 p.u. while the PI presents significantly larger deviations up to 4.2 % in the last step change. To enable a better visualization of the differences between the responses of the controllers, a zoom corresponding to the first step change of the active power response is shown from 4.5 to 7 s.

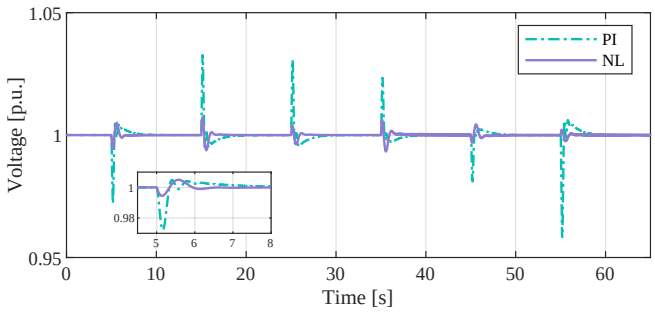

Fig. 8: Terminal voltage magnitude response when the active power is subjected to a sequence of reference step changes.

Finally, as suggested by the converter energy model in (18), a change in active power results in a disturbance in the converter energy. Fig. 9 shows the converter energy behavior when the active power reference is subjected to a series of step changes.

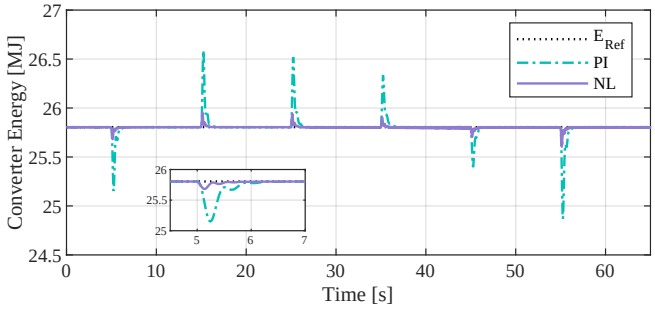

Fig. 9: Converter energy response when the active power is subjected to a sequence of reference step changes.

The NL controller is able to reject the disturbances in the converter energy as well. Due to the full consideration of the interactions between the converter state variables, the NL controller presents a better performance in rejecting the disturbances originated from the sequence of step changes to the active power as it can be seen in the zoom shown within Fig. 9. Overall, the NL controller kept the converter energy within a ± 0.7 % range from its reference value whilst the PI controller exhibited a variation within the ± 3.6 % range.

The analysis of Figs. 8 and 9 show the main advantage in using the proposed NL controller despite the similar performances seen in the results shown by Figs. 6 and 7. The design of the proposed NL controller does not rely on a single operating point as does the PI controller. The latter is obtained from a linearized model around the starting operating point whose accuracy in representing the system dynamics is limited to the vicinity of the point of linearization. Therefore, the proposed NL controller is able to retain the desired performance around any operation point within the converter physical limits.

B. Converter Energy Reference Tracking

The second evaluated scenario is the capability of the control system to follow step changes in the converter energy reference value. The interest behind following a dynamic change in the energy reference value can be seen in [29] where the converter energy is modulated to act as a buffer between the AC and DC sides of the converter. The results shown in this section are for a scenario where the MMC is injecting 0.6 p.u. of active power into the electric grid.

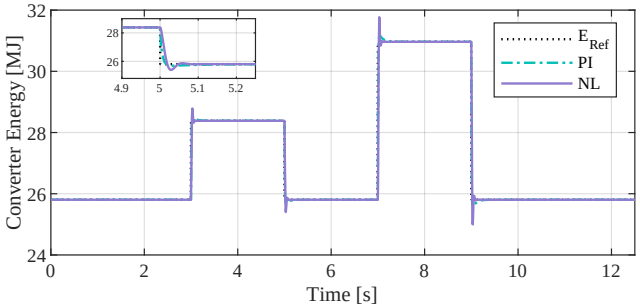

Fig. 10: Converter energy response following a sequence of step changes to its reference value

The converter energy response following two step changes of 10 % and 20 % is shown in Fig. 10. The MMC station equipped with the proposed NL controller is able to track the changing converter energy reference with a settling time of nearly 0.1 s. For comparison purposes, the same reference change was applied to the test system also considering that the MMC station is embedded with a PI controller. The difference between the controllers responses shown in Fig. 10 is subtle and can be analyzed by zooming in each step. Fig. 10 also shows the zoom around the energy response to the step change applied at t =3 s where we can see the main differences between the response of the controllers. It can be seen that the initial response of the PI controller is faster. However, the NL controller response is less damped, showing a small overshoot. Also, the NL controller settles 0.1 s faster to the new reference value than the PI controller.

Despite the responses of the converter energy when adopting the NL and the PI controller being similar, their impact in the control effort has a bigger difference. Fig. 11 shows the trajectories of the 0-component of the circulating current for both cases.

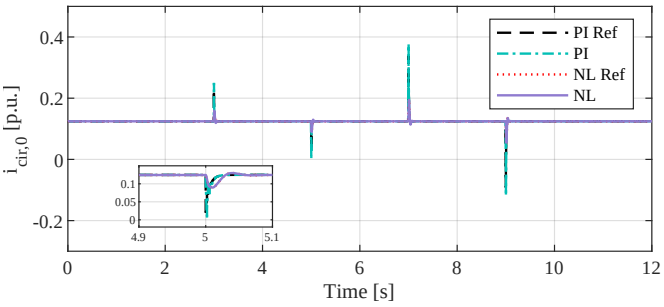

Fig. 11: 0-component of the circulating current response following the step changes applied to the converter energy reference value.

We can see that the NL controller is able to achieve a fast control of the converter energy through smaller changes on the $i^*_{cir,0}$ trajectory. Whilst the NL controller keeps the trajectory within ± 56 % of the equilibrium value, the PI controller

presents significantly larger excursion of ±200 %. Another interesting fact is that the PI controller requires the power flow in the DC side to be reversed momentarily as the 0-component of the circulating current crosses zero at t =9 s.

Finally, Fig. 11 also shows a zoom in the circulating current for the step applied at $t = 5$ s to complement the analysis of the zoom shown in Fig. 10. The differences between the energy responses can be seen in how they generate the trajectory for the 0-component of the circulating current. To achieve the response shown in Fig. 10, the NL controller achieves the response with a smoother change of the 0-component of the circulating current whilst the PI controller has a greater deviation form the steady-state value. The better performance shown by the NL controller in terms of control effort is also attributed to the fact that the controller is designed considering the nonlinearities of the converter dynamics. We note from (18) that the converter energy dynamics is highly nonlinear in respect to the converter's inputs and state variables. The developed NL controller does not neglect the interactions from other state variables resulting in a controller that is capable of achieving a fast response with less disturbances in the circulating current 0-component.

C. Controller Performance During Frequency Support

The last evaluation scenario considered in this work is regarding the controller performance during a contingency that demands frequency support from the MMC. The active power for the converter is 30 % of the total load of the test system, meaning that the scenario considered has a high penetration of non-synchronous generation. To simulate a frequency disturbance, the load shown in Fig. 3 is suddenly increased from 2000 MW to 2500 MW, which represents an increase of 25 %.

Fig. 12 shows the frequency response of the system in the considered scenario. When the NL controller is used, the test system presented a slightly smaller deviation from the rated value of 60 Hz in comparison to when the PI controller is adopted. Also, when the NL controller is used, the system settles 3 s faster to the new equilibrium point after the disturbance.

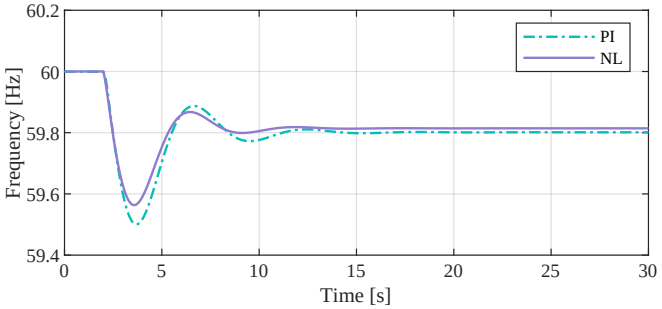

Fig. 12: Frequency response of the test system to a sudden 25 % load increase.

More critically, the NL controller presented a smaller frequency nadir, meaning that the maximum frequency deviation of 0.436 Hz was smaller than when using the PI controller that deviated 0.5 Hz from the rated frequency value. The frequency nadir and the rate of change of frequency are crucial values for tuning the protection equipment. Having smaller values for these parameters means that the system could avoid losing further generation if the protection relays were set at $59.55Hz$.

The frequency support is performed by injecting active power in the system to counteract a frequency dip as is the case in the studied scenario. The active power response is shown in Fig. 13. The NL controller is able to react slightly quicker than the PI controller, resulting in slightly more power (0.02 p.u., as seen in the final seconds of the simulation) of the extra load been allocated to the MMC-HVDC due to the power sharing mechanism with the grid equivalent of Fig. 3.

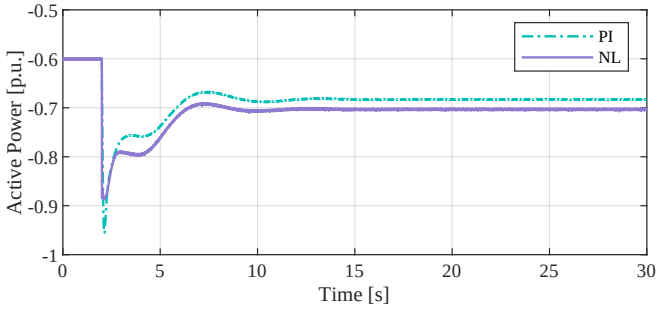

Fig. 13: Active power response of the MMC following the sudden 25 % load increase.

As shown in section V-A, a disturbance is introduced in the terminal voltage in the dq frame when there is a sudden change in the converter frequency. The magnitude of the output voltage is shown in Fig. 14. The proposed NL controller is able to reject the disturbance cause by the frequency variation. Moreover, when using the NL controller, the terminal voltage presents a similar settling time to the one obtained using the PI of 1.5 s . However, with the NL controller, the voltage dip is 6 % smaller than with the PI, and the following overshoot is 0.8 % smaller.

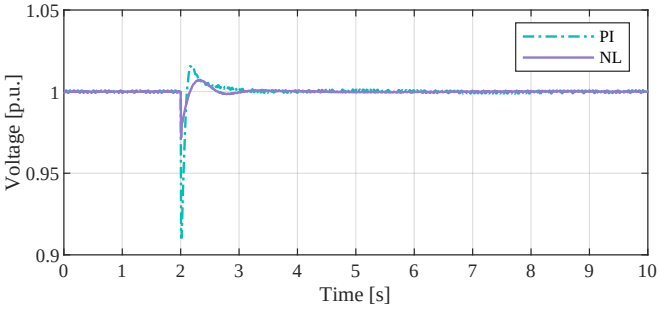

Fig. 14: Absolute value of the output voltage response of the MMC following the sudden 25 % load increase.

Finally, change in active power to provide frequency response results in a disturbance to the converter energy. The energy response is shown in Fig. 15.

The proposed NL controller is able to reject the disturbance in the converter energy to a maximum drop of 2.7 %. For comparison, the PI controller presents a maximum deviation of 3.8 % in the converter energy. Moreover, the NL controller is able to reject this disturbance 1 s faster than the PI controller. The better performance of the proposed NL controller was

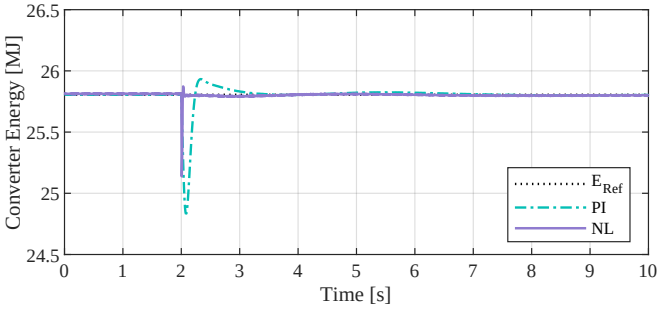

Fig. 15: Converter energy response of the MMC following the sudden 25 % load increase.

expected in this scenario since it considers the interaction between all state variables and inputs of the MMC station model. It is worth pointing out that the ever changing conditions of the power system allied with the frequent disturbances caused in the system such as the connection/disconnection of big loads, the unavailability of transmission lines and loss of generation, a controller as the one proposed in this work that is best suited for dealing with such sudden changes is desirable.

VI. Conclusions

In this paper we present a nonlinear controller for MMCs that is compatible with GFM converter operation, thus providing frequency support and synthetic inertia to the AC grid where it is connected. The controller is designed following feedback linearization and dynamic feedback linearization principles. Furthermore, we present a detailed mathematical stability analysis using Lyapunov theory and demonstrate that the system is asymptotically stable. To validate the proposed controller, a test system is implemented using Matlab/Simscape Electrical and three scenarios are evaluated: active power reference tracking, converter energy reference tracking and the provision of frequency support. The proposed nonlinear controller presents a good performance in tracking the reference signals and rejecting the disturbances that arise from the high degree of interconnection of the system's variables. Finally, the proposed nonlinear controller presents a better performance than a classic PI controller whilst ensuring better disturbance rejection and less control effort. In future works, since the MMC is able to performe as a GFM converter, it will be studied the design of additional control layers, such as to provide further ancillary services to the AC grid. Among others, if reserves are available, it can be studied the possibility of including fast frequency support (sub second) and Frequency Containment Reserve (primary support), and reactive power provision.

Acknowledgment

The authors thank the anonymous Reviewers and the Associate Editor for their comments that improved the paper's quality.

The authors would like to thank the São Paulo Research Foundation FAPESP (grant#2021/10421-0 and #2023/00682-6), the National Council for Scientific and Technological Development CNPq (grant#407867/2022-8) and the French National Research Agency ANR (grant ESTHER ANR-22-CE05-0016) for supporting this research.

References

[1] J. C. Gonzalez-Torres, V. Costan, G. Damm, A. Benchaib, A. Bertinato, S. Poullain, B. Luscan, and F. Lamnabhi-Lagarrigue, "Hvdc protection criteria for transient stability of ac systems with embedded hvdc links," *The Journal of Engineering*, vol. 2018, no. 15, pp. 956–960, 2018.

[2] Y. Chen, M. J. Carrizosa, G. Damm, F. Lamnabhi-Lagarrigue, M. Li, and Y. Li, "Control-induced time-scale separation for multiterminal high-voltage direct current systems using droop control," *IEEE Transactions on Control Systems Technology*, vol. 28, no. 3, pp. 967–983, 2019.

[3] M. P. Bahrman and B. K. Johnson, "The abcs of hvdc transmission technologies," *IEEE power and energy magazine*, vol. 5, no. 2, pp. 32–44, 2007.

[4] A. Lesnicar and R. Marquardt, "An innovative modular multilevel converter topology suitable for a wide power range," in *2003 IEEE Bologna Power Tech Conference Proceedings,*, vol. 3. IEEE, 2003, pp. 6–pp.

[5] M. Glinka and R. Marquardt, "A new ac/ac multilevel converter family," *IEEE Transactions on Industrial Electronics*, vol. 52, no. 3, pp. 662–669, 2005.

[6] R. Marquardt, "Modular multilevel converter: An universal concept for hvdc-networks and extended dc-bus-applications," in *The 2010 International Power Electronics Conference-ECCE ASIA-*. IEEE, 2010, pp. 502–507.

[7] O. Gomis-Bellmunt, J. Sau-Bassols, E. Prieto-Araujo, and M. Cheah-Mane, "Flexible converters for meshed hvdc grids: From flexible ac transmission systems (facts) to flexible dc grids," *IEEE Transactions on Power Delivery*, vol. 35, no. 1, pp. 2–15, 2020.

[8] J. Peralta, H. Saad, S. Dennetière, J. Mahseredjian, and S. Nguefeu, "Detailed and averaged models for a 401-level mmc–hvdc system," *IEEE Transactions on Power Delivery*, vol. 27, no. 3, pp. 1501–1508, 2012.

[9] S. Debnath, J. Qin, B. Bahrani, M. Saeedifard, and P. Barbosa, "Operation, control, and applications of the modular multilevel converter: A review," *IEEE transactions on power electronics*, vol. 30, no. 1, pp. 37–53, 2014.

[10] H. Saad, S. Dennetière, J. Mahseredjian, P. Delarue, X. Guillaud, J. Peralta, and S. Nguefeu, "Modular multilevel converter models for electromagnetic transients," *IEEE Transactions on Power Delivery*, vol. 29, no. 3, pp. 1481–1489, 2013.

[11] L. Meegahapola, A. Sguarezi, J. S. Bryant, M. Gu, E. R. Conde D, R. Cunha *et al.*, "Power system stability with power-electronic converter interfaced renewable power generation: Present issues and future trends," *Energies*, vol. 13, no. 13, p. 3441, 2020.

[12] F. Milano, F. Dörfler, G. Hug, D. J. Hill, and G. Verbič, "Foundations and challenges of low-inertia systems," in *2018 Power Systems Computation Conference (PSCC)*. IEEE, 2018, pp. 1–25.

[13] "Preliminary report: black system event in south australia on 28 september 2016," Australian Energy Market Operator, Tech. Rep., 2016.

[14] "All-island generation capacity statement 2017-2026," EirGrid and SONI, Tech. Rep., 2017. [Online]. Available: http://www.eirgridgroup.com

[15] P. Du, N. V. Mago, W. Li, S. Sharma, Q. Hu, and T. Ding, "New ancillary service market for ercot," *IEEE Access*, vol. 8, pp. 178 391–178 401, 2020.

[16] "9 august 2019 power outage report," OFGEM, Tech. Rep., 2019.

[17] "Stability management in power electronics dominated systems: A prerequisite to the success of the energy transition," ENTSO-E, Tech. Rep., 2022. [Online]. Available: https://www.entsoe.eu/news/2022/06/21/entso-e-publishes-a-position-paper-on-stability-management-in-power-electronics-dominated-systems/

[18] J. Matevosyan, B. Badrzadeh, T. Prevost, E. Quitmann, D. Ramasubramanian, H. Urdal, S. Achilles, J. MacDowell, S. H. Huang, V. Vital *et al.*, "Grid-forming inverters: Are they the key for high renewable penetration?" *IEEE Power and Energy magazine*, vol. 17, no. 6, pp. 89–98, 2019.

[19] R. Musca, A. Vasile, and G. Zizzo, "Grid-forming converters. a critical review of pilot projects and demonstrators," *Renewable and Sustainable Energy Reviews*, vol. 165, p. 112551, 2022.

[20] G. Denis, T. Prevost, M.-S. Debry, F. Xavier, X. Guillaud, and A. Menze, "The migrate project: the challenges of operating a transmission grid with only inverter-based generation. a grid-forming control improvement with transient current-limiting control," *IET Renewable Power Generation*, vol. 12, no. 5, pp. 523–529, 2018.

[21] J. Chen, M. Liu, F. Milano, and T. O'Donnell, "100% converter-interfaced generation using virtual synchronous generator control: A case study based on the irish system," *Electric Power Systems Research*, vol. 187, p. 106475, 2020.

[22] M. Ndreko, S. Rüberg, and W. Winter, "Grid forming control scheme for power systems with up to 100% power electronic interfaced generation: a case study on great britain test system," *IET Renewable Power Generation*, vol. 14, no. 8, pp. 1268–1281, 2020.

[23] Q.-C. Zhong and G. Weiss, "Synchronverters: Inverters that mimic synchronous generators," *IEEE transactions on industrial electronics*, vol. 58, no. 4, pp. 1259–1267, 2010.

[24] S. D'Arco, J. A. Suul, and O. B. Fosso, "Small-signal modeling and parametric sensitivity of a virtual synchronous machine in islanded operation," *International Journal of Electrical Power & Energy Systems*, vol. 72, pp. 3–15, 2015.

[25] ——, "A virtual synchronous machine implementation for distributed control of power converters in smartgrids," *Electric Power Systems Research*, vol. 122, pp. 180–197, 2015.

[26] A. Tayyebi, A. Anta, and F. Dörfler, "Grid-forming hybrid angle control and almost global stability of the dc-ac power converter," *IEEE Transactions on Automatic Control*, 2022.

[27] I. Subotić and D. Groß, "Power-balancing dual-port grid-forming power converter control for renewable integration and hybrid ac/dc power systems," *IEEE Transactions on Control of Network Systems*, 2022.

[28] J. Erdocia, A. Urtasun, and L. Marroyo, "Power angle–frequency droop control to enhance transient stability of grid–forming inverters under voltage dips," *IEEE Journal of Emerging and Selected Topics in Power Electronics*, 2022.

[29] E. Sánchez-Sánchez, E. Prieto-Araujo, and O. Gomis-Bellmunt, "The role of the internal energy in mmcs operating in grid-forming mode," *IEEE Journal of Emerging and Selected Topics in Power Electronics*, vol. 8, no. 2, pp. 949–962, 2019.

[30] M. Guan, W. Pan, J. Zhang, Q. Hao, J. Cheng, and X. Zheng, "Synchronous generator emulation control strategy for voltage source converter (vsc) stations," *IEEE Transactions on Power Systems*, vol. 30, no. 6, pp. 3093–3101, 2015.

[31] Z. Lv and Q.-C. Zhong, "Control of modular multilevel converters as virtual synchronous machines," in *2017 IEEE Power & Energy Society General Meeting*. IEEE, 2017, pp. 1–5.

[32] S. D'Arco, G. Guidi, and J. A. Suul, "Operation of a modular multilevel converter controlled as a virtual synchronous machine," in *2018 International Power Electronics Conference (IPEC-Niigata 2018-ECCE Asia)*. IEEE, 2018, pp. 782–789.

[33] H. Saad, P. Rault, and S. Dennetière, "Investigation on parallel operation of two mmc-hvdc links in grid forming connected to an existing network," in *2020 22nd European Conference on Power Electronics and Applications (EPE'20 ECCE Europe)*. IEEE, 2020, pp. P–1.

[34] E. Sánchez-Sánchez, E. Prieto-Araujo, A. Junyent-Ferré, and O. Gomis-Bellmunt, "Analysis of mmc energy-based control structures for vsc-hvdc links," *IEEE Journal of Emerging and Selected Topics in Power Electronics*, vol. 6, no. 3, pp. 1065–1076, 2018.

[35] E. Rokrok, T. Qoria, A. Bruyere, B. Francois, H. Zhang, M. Belhaouane, and X. Guillaud, "Impact of grid-forming control on the internal energy of a modular multilevel converter," in *2020 22nd European Conference on Power Electronics and Applications (EPE'20 ECCE Europe)*. IEEE, 2020, pp. 1–10.

[36] S. Yang, P. Wang, and Y. Tang, "Feedback linearization-based current control strategy for modular multilevel converters," *IEEE Transactions on Power Electronics*, vol. 33, no. 1, pp. 161–174, 2017.

[37] G. C. de Oliveira, G. Damm, R. M. Monaro, L. F. Lourenço, M. J. Carrizosa, and F. Lamnabhi-Lagarrigue, "Nonlinear control for modular multilevel converters with enhanced stability region and arbitrary closed loop dynamics," *International Journal of Electrical Power & Energy Systems*, vol. 126, p. 106590, 2021.

[38] M. Ahmadijokani, M. Mehrasa, M. Sleiman, M. Sharifzadeh, A. Sheikholeslami, and K. Al-Haddad, "A back-stepping control method for modular multilevel converters," *IEEE Transactions on Industrial Electronics*, vol. 68, no. 1, pp. 443–453, 2020.

[39] P.-B. Steckler, J.-Y. Gauthier, X. Lin-Shi, and F. Wallart, "Differential flatness-based, full-order nonlinear control of a modular multilevel converter (mmc)," *IEEE Transactions on Control Systems Technology*, 2021.

[40] "Review of relevance of current techniques to advanced frequency control," RESERVE, Tech. Rep., 2017.

[41] M. Vatani, M. Hovd, and M. Saeedifard, "Control of the modular multilevel converter based on a discrete-time bilinear model using the sum of squares decomposition method," *IEEE Transactions on Power Delivery*, vol. 30, no. 5, pp. 2179–2188, 2015.

[42] K. Sharifabadi, L. Harnefors, H.-P. Nee, S. Norrga, and R. Teodorescu, *Design, control, and application of modular multilevel converters for HVDC transmission systems*. John Wiley & Sons, 2016.

[43] M. Pai, *Energy function analysis for power system stability*. Springer Science & Business Media, 1989.

[44] H. K. Khalil and J. W. Grizzle, *Nonlinear systems*. Prentice hall Upper Saddle River, NJ, 2002, vol. 3.

[45] P. Rouchon, "Necessary condition and genericity of dynamic feedback linearization," *J. Math. Systems Estim. Control*, vol. 4, no. 2, pp. 257–260, 1994.

[46] F. Perez, A. Iovine, G. Damm, L. Galai-Dol, and P. F. Ribeiro, "Stability analysis of a dc microgrid for a smart railway station integrating renewable sources," *IEEE Transactions on Control Systems Technology*, vol. 28, no. 5, pp. 1802–1816, 2019.

[47] Y. Chen, G. Damm, A. Benchaib, M. Netto, and F. Lamnabhi-Lagarrigue, "Control induced explicit time-scale separation to attain dc voltage stability for a vsc-hvdc terminal," *IFAC Proceedings Volumes*, vol. 47, no. 3, pp. 540–545, 2014.

[48] J. C. Gonzalez-Torres, G. Damm, V. Costan, A. Benchaib, and F. Lamnabhi-Lagarrigue, "Transient stability of power systems with embedded vsc-hvdc links: Stability margins analysis and control," *IET Generation, Transmission & Distribution*, vol. 14, no. 17, pp. 3377–3388, 2020.

[49] Q. Guo, M. Jiménez Carrizosa, A. Iovine, and A. Arzandé, "Dynamic Feedback Linearization and Singular Perturbation for a Stabilizing Controller for DC/DC Boost Converters: Theory and Experimental Validation," *IEEE Transactions on Industrial Electronics*, vol. 71, no. 8, pp. 9559–9568, 2024.

[50] A. Yazdani and R. Iravani, *Voltage-sourced converters in power systems: modeling, control, and applications*. John Wiley & Sons, 2010.

Luís F. Normandia Lourenço received the Ph.D. degree in electrical engineering from the Polytechnic School of the University of São Paulo (USP), Brazil, in 2022. In 2021, he was a Visiting Ph.D. Student at the Laboratoire des Signaux et Systèmes (L2S), CentraleSupélec, University Paris-Saclay, France. Since 2023, he is an Associate Professor at the Institute of Energy and Environment of the University of São Paulo (IEE-USP). His research interests focus on grid-forming converters, renewable energy integration, HVDC transmission systems, microgrids, control and stability of power systems, and applied nonlinear control.

Alessio Iovine (M'18) received the B.Sc. and M.Sc. degrees in electrical engineering and computer science from the University of L'Aquila, L'Aquila, Italy, in 2010 and 2012, respectively, and the European Doctorate degree in information science and engineering in 2016 from the University of L'Aquila, L'Aquila, Italy, in collaboration with CentraleSupélec, Paris-Saclay University, Gif-sur-Yvette, France. From 2016 to 2020, he held Post-Doctoral positions at University of L'Aquila, Efficacity Research Center (France), University of California at Berkeley (USA), and CentraleSupélec. In 2020, he joined the CNRS as Researcher and is with the L2S, Paris-Saclay University. Dr. Iovine has co-authored more than 50 papers covering advanced control methods for power and energy systems as well as traffic control ones, with smart grids and autonomous vehicles as core applications. He is a member of the IFAC Technical Committee TC 6.3 Power and Energy Systems since 2020.

His research interests focus on control methods for cyber-physical systems, particularly in the modeling and control of large-scale systems and optimal multi-level information management. Recently, he has concentrated on developing optimal control strategies to improve the integration and utilization of renewables and storage devices in power systems, as well as reducing consumption and maximizing traffic throughput in cooperative intelligent transportation systems.

Gilney Damm is a Senior Research Scientist (Directeur de Recherche) at University Gustave Eiffel, at the Laboratoire COSYS-IMSE. Previously he was an Associate Professor at the Paris-Saclay University, CentraleSupelec, France. He is an Electronic Engineer – Automatic Control from the Rio de Janeiro Federal University – Brazil, and PhD from CentraleSupelec - Paris-Saclay University. His research interests concern nonlinear and adaptive control and observers applied to power systems (SmartGrids, SuperGrid, MicroGrids). His main applications are in the field of large-scale integration of renewable energy and electric vehicles; Multi-Terminal HVDC systems; Mixed AC/DC MicroGrids; Control of Power Systems and Power Electronics in high and low voltage, AC and DC (transient stabilization, frequency, and voltage stability, synthetic inertia, grid forming converters); synchronization of power networks; energy integration in SmartCities; Dynamic recharging of electric vehicles (along the road). He has a large experience as a coordinator or Work-Package Leader in several European and French research projects, in particular the Institutes for Energy Transition SuperGrid (on large-scale high voltage electrical grids), Efficacity (on MicroGrids and SmartCities) and Vedecom (on dynamic inductive charging of electric vehicles). He is a member of the IFAC Technical Committee TC 6.3 Power and Energy Systems since 2015. He has been Associate Editor at the European Journal of Control since 2010 and Energies since 2020.

Alfeu J. Sguarezi Filho received his Master and Doctor degrees in Electrical Engineering from the Faculty of Electrical and Computer Engineering of the University of Campinas (Unicamp) in 2007 and 2010, respectively. Currently, he is Associate Professor at the Federal University of ABC (UFABC). He is a Senior Member of the IEEE and author of several articles in national and international scientific journals and book chapters in the areas of electrical machines, machine drives, electric vehicles, power electronics, wind and photovoltaic energies.